Sustainable Energy & Fuels

ZIF-67-derived edge-oriented graphene clusters coupled with carbon nanotubes containing encapsulated Co nanoparticles for high-frequency electrochemical capacitors

Journal:	*Sustainable Energy & Fuels*
Manuscript ID	SE-ART-07-2019-000503.R1
Article Type:	Paper
Date Submitted by the Author:	15-Aug-2019
Complete List of Authors:	Li, Wenyue; Texas Tech University, Department of Electrical and Computer Engineering Islam, Nazifah; BaoNano LLC Azam, Sakibul; Texas Tech University, Nano Tech Center and Department of Electrical and Computer Engineering Xu, Zhen; Texas Tech University Warzywoda, Juliusz; Texas Tech University, Fan, Zhaoyang; Texas Tech University,

ZIF-67-derived edge-oriented graphene clusters coupled with carbon nanotubes containing encapsulated Co nanoparticles for high-frequency electrochemical capacitors

Wenyue Li[a], Nazifah Islam[b], SakibulAzam[a], Zhen Xu[a], Juliusz Warzywoda[c], and Zhaoyang Fan[a]*

[a] *Department of Electrical and Computer Engineering and Nano Tech Center, Texas Tech University, Lubbock, Texas, 79409, USA*

[b] *BaoNano, LLC, Lubbock, Texas, 79415, USA*

[c]*Materials Characterization Center, Whitacre College of Engineering, Texas Tech University, Lubbock, TX 79409, USA*

** Email: zhaoyang.fan@ttu.edu*

Abstract

There is a strong interest in increasing frequency response of the electrochemical capacitors (ECs) from typically less than 1 Hz to the hundreds or the kilo Hz range, so that such high-frequency ECs (HF-ECs) could replace conventional capacitors for AC line-frequency filtering and other capacitor applications. The development of such HF-ECs is hindered by their typically low capacitance density and operation voltage. Herein, by treating ZIF-67 particulate films in CH_4/H_2 plasma, edge-oriented graphene (EOG) formed around the carbonized ZIF-67 particulate skeleton, and this EOG was coupled with carbon nanotubes (CNTs) that were grown with the aid of Co catalyst nanoparticles, which were generated

by reducing the Co^{2+} ions associated with ZIF in the plasma. Used as electrodes, these EOG/CNT/carbonized ZIF-67 composites exhibited a large electrode areal capacitance of 1.0 mF cm^{-2} and an excellent frequency response of -84° phase angle at 120 Hz in aqueous electrolyte cells, whereas values of 0.67 mF cm^{-2} and -78° for the electrode areal capacitance and the phase angle at 120 Hz, respectively, were obtained in organic electrolyte cells with the operation voltage of 2.5 V. Using three pairs of electrodes stacked together, a single integrated cell operating at 7.5 V and having a characteristic frequency of ~3.8 KHz at -45° phase angle, was demonstrated. These results suggest the potential to use this EOG/CNT/carbonized ZIF-67 composite structure for developing HF-ECs.

Keywords: metal organic framework, oriented graphene, carbon nanotube, electrochemical capacitor, AC-filtering

Introduction

Conventional electrochemical capacitors (ECs) or supercapacitors are normally employed in low frequency devices (up to ~1 Hz) because of their limited capability to handle fast charge-discharge rates. So it is highly desirable to increase this frequency to the hundreds or the kilo hertz regime so that such high-frequency ECs (HF-ECs), with a high capacitance density, can replace bulky aluminum electrolytic capacitors (AECs) for current ripple filtering, pulse power generation and storage, and other applications, thus expanding the application scope of ECs.[1-2]

In a conventional EC using mesoporous carbon electrodes, the limited electrolyte ion transportation rate in the mesoporous structure determines how fast the electrical double layer can be formed deep in the pores, thus the capacitance inevitably decreases significantly as the frequency increases to only a few hertz. Minimizing the porous effect by adopting straightforward and large-size pores that make the electrodes easily impregnate by the electrolytes, minimizing the equivalent series resistance (ESR) by enhancing electrode material's conductivity, and eliminating the contact resistance between the electrode material and the current collector, are the key design guidelines toward developing HF-ECs. So far, most of the studies on HF-EC electrodes were focused on the carbon-based materials such as graphene,[3-11] carbon nanotubes (CNTs),[12-15] carbon fibers,[16] carbon black,[17] and composites based on the aforementioned elements,[18-19] because of their tunable structures being absent of micro-, dead or tortuous pores. Poly(3,4-ethylenedioxythiophene) (PEDOT)-based conductive polymers[20] and most recently

MXene[21-22] and other 2D nanostructures[23] also show a very promising electrochemical performance for HF-ECs.

Different from dielectric-based AECs, whose operational voltage depends on the thickness of the aluminum oxide layer that is electrochemically formed on the etched aluminum foil,[2] electrical double layer-based HF-ECs have small potential windows that are limited by the decomposition of the employed electrolyte. Since the ionic conductivity of aqueous electrolyte is much higher than that of organic electrolyte, the frequency response and the capacitance of an aqueous cell will be much better than those of an organic cell when the same electrodes are used. Therefore, most HF-ECs reported in the literature employed aqueous electrolyte, which has a maximum voltage restricted to ~0.9 V, whereas an organic electrolyte cell may be used at a voltage larger than 2.5 V.[24-27] In practice, since a filtering capacitor typically runs at a voltage no smaller than several volts, multiple cells must be used in series. Considering that the goal of developing HF-ECs to replace electrolytic capacitors is mainly driven by miniaturization of device size, much more attention should be paid to the organic electrolyte-based HF-ECs. Even for the organic cells, for practical applications multiple cells must be integrated into one package to form a single miniaturized HF-EC device with a reasonable voltage window. It is known that with a series connection, the ESR will proportionally increase while the capacitance will decrease at the same ratio. All these factors necessitate the electrode materials to have better performance. To the best of our knowledge, there has been very limited studies on integrating multiple cells into one package to fabricate HF-ECs with a higher voltage

window[28], except the study that connected several packaged cells in an external circuit,[29] which clearly has no merits when compared to a single AEC.

Oriented graphene structures, either vertically oriented graphene (VOG) on a flat substrate[1, 3] or edge-oriented graphene (EOG) encircling a metal- or carbon-formed 3D structure,[5, 30] have been widely reported for HF-ECs. We expect that if EOG could be grown around 1-2 μm microscale skeleton that forms a 3D structure, the areal capacitance density, in terms of the per footprint of the device, might be further increased. In this paper, EOG wrapped around the carbonized ZIF-67 skeleton and coupled with CNTs, is investigated as an electrode structure for HF-ECs. This structure is synthesized by first growing zeolitic imidazolate framework-67 (ZIF-67) on stainless steel (SS) current collector, and then treating this product in H_2/CH_4 plasma for a few minutes *via* the microwave plasma enhanced chemical vapor deposition (PECVD) method. Carbonization of ZIF-67 in this plasma environment not only maintains the polyhedral morphology of ZIF-67 and reduces the Co^{2+} ions to conductive Co nanoparticles (NPs), but also introduces EOG flakes wrapped around the carbonized ZIF-67 skeleton and forms CNTs utilizing Co NPs. This structure provides both a high conductivity and abundant sites for electrolytic ions to adsorb. As a result, the composite electrodes showed a characteristic frequency of 3.2 KHz at -45° phase angle and the areal capacitance (C_A) of ~1.0 mF cm^{-2} at 120 Hz in 6 M aqueous KOH electrolyte. The testing voltage was further extended to 2.5 V by using 1 M tetraethylammonium tetrafluoroborate ($TEABF_4$) in acetonitrile electrolyte and 7.5 V by integrating three pairs of electrodes in one package. Particularly, this 7.5 V HF-EC

shows very competitive electrochemical performance with a phase angle of -72^{o} at 120 Hz, making this structure very promising in practical applications.

Results and Discussion

Figure 1(a) schematically illustrates the electrode preparation process and the resulting structures of carbonized ZIF (C-ZIF) samples prepared with or without direct exposure to CH_4/H_2 plasma. ZIF-67 films were synthesized on SS disks used as substrates in a wetchemistry process using separate methanolic solutions of 2-methylimidazole and cobalt nitrate hexahydrate. After coating with ZIF-67, SS disks exhibited the characteristic purple color of ZIF-67 (Figure S1 in the Supplementary Information, SI). The polyhedral morphology and size (~1-2 μm) of as-synthesized ZIF-67 microparticles is shown in scanning electron microscope (SEM) images in Figure S2(a, b).

The ZIF-67 films were subsequently treated in a high-temperature CH_4/H_2 plasma in a PECVD system. After this treatment, the sample exhibited black color (Figure S1). Different plasma treatment durations, 3, 5 and 8 minutes, were applied to study the structural evolution of products, and the resulting samples are designated as C-ZIF/SS-3, C-ZIF/SS-5 and C-ZIF/SS-8, respectively. For comparison, the ZIF-67 film was also sandwiched between two graphite sheets to avoid the direct exposure of this film to the plasma species, and then carbonized under the same plasma conditions for 5 minutes. This sample, obtained by thermal carbonization, is designated as C-ZIF/SS.

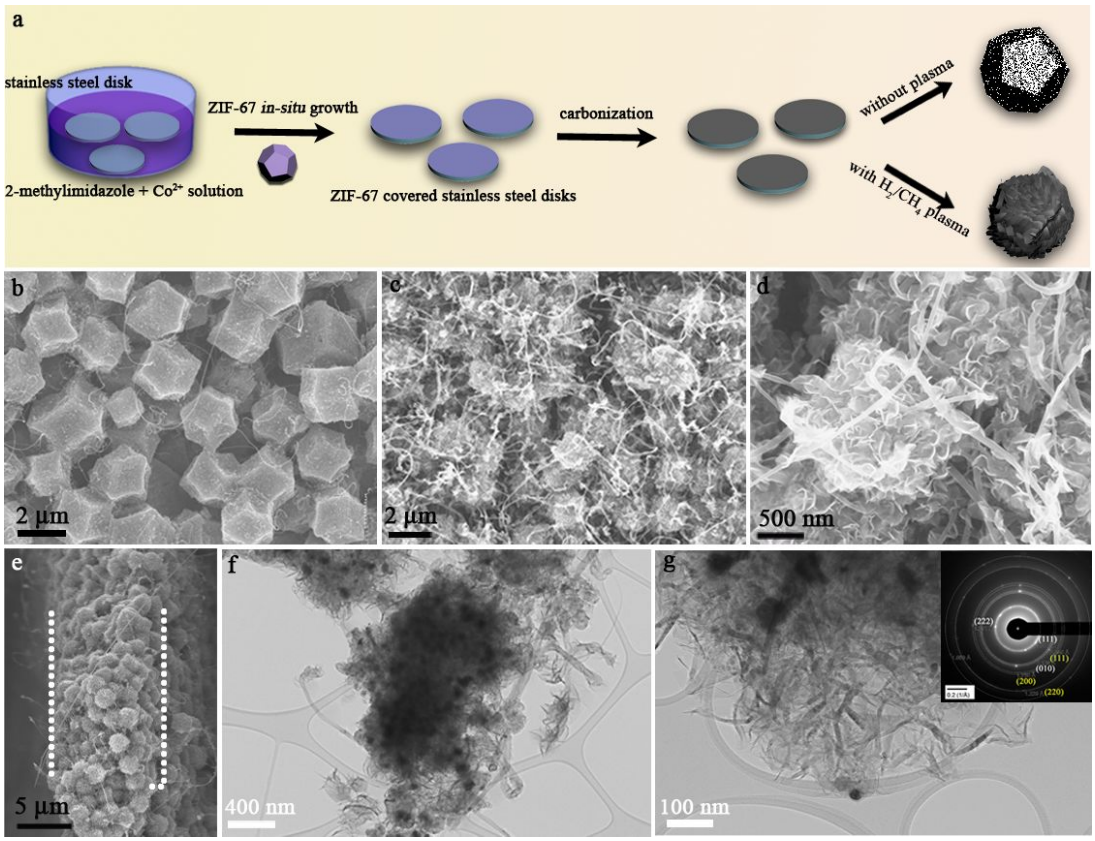

Figure 1. Schematic illustration of the electrode preparation process (a). SEM images of samples C-ZIF/SS (b)and C-ZIF/SS-5 (c, d). SEM image of the C-ZIF/SS-5sample cross-section (e). TEM image of Co NPs on/near two C-ZIF-67 particles (f).TEM image of EOG flakes formed around C-ZIF-67particles (g). The inset of (g) depicts the SAED pattern of the EOG/CNT/C-ZIF composite.

As shown in Figures 1(b) and S2(c, d) for sample C-ZIF/SS, the polyhedral morphology of ZIF-67 is well preserved after thermal carbonization, and the rough-appearing/specked surface of ZIF-67 after thermal carbonization suggests formation of Co NPs. This is similar to the reported structures of thermally carbonized ZIF-67 materials.[31-32] The catalytic effect of Co NPs promoted the growth of sparse long CNTs in sample C-

ZIF/SS (Figures 1(b) and S2 (c, d)) from the adventitious carbon species in the plasma even though this sample was shielded from the direct plasma exposure. In contrast, samples that were directly exposed to the plasma had different morphologies. For sample C-ZIF/SS-3 (Figure S3(a-c)), the polyhedral morphology of the as-synthesized ZIF-67 was also maintained but dense EOG flakes and sparse CNTs were wrapped around C-ZIF-67 polyhedrons. After 5 minutes of plasma treatment, abundant tangled CNTs appeared throughout the EOG-encaged C-ZIF-67 polyhedrons in sample C-ZIF/SS-5 (Figures 1(c, d) and S3(d-f)). Interestingly, some of these CNTs were also modified by EOG deposition. The cross-section image of sample C-ZIF/SS-5, shown in Figure 1(e), demonstrates a compact multilayered structure with the whole layer thickness of ~7 μm. This image also shows that in addition to being present on the top surface of C-ZIF film, EOG was deposited uniformly throughout the entire film. With such an architecture formed by the interspersed EOG, CNTs and C-ZIF polyhedrons, fast electron transfer pathways are provided, and oriented EOG flakes can simultaneously facilitate electrolytic ion transportation. However, in contrast to the reported vertical graphene formed on metal foils, this architecture is expected to exhibit a reasonably high specific surface area for a large capacitance. These features should provide a quick frequency response and a large capacitance for HF-EC applications. As shown in Figure S3(g-i), prolonging the plasma exposure time to 8 minutes resulted in a dense EOG deposition on CNTs; thus, EOG became the dominate surface feature for sample C-ZIF/SS-8. The morphological and structural characteristics of the EOG/CNT/C-ZIF composite were further elucidated using

transmission electron microscopy (TEM), high-resolution TEM (HRTEM), and selected area electron diffraction (SAED) (Figures 1(f, g) andS4)). In addition to graphene and CNTs, NPs encapsulated in a graphitic carbon shell were clearly observed by TEM and HRTEM. The inset of Figure 1(g) presents two sets of diffraction patterns (DPs). One DP (shown in white color) can be assigned to (111), (222) and (010) crystal planes of graphite; the other DP (shown in yellow color) can be assigned to (111), (200) and (220) crystal planes of metallic Co with fcc structure.[33-34] The edge-oriented structure of graphene is clearly shown in Figure S4(b), which reveals tapered profile of EOG with narrow tip. Based on the structural evolution caused by different plasma exposure times for these four samples, the growth mechanism for this unique structure can be proposed. As it is carbonized in the plasma, ZIF-67 serves as a template for EOG growth around its surfaces, and at the same time ZIF-67 provides the cobalt source for the formation of Co NPs in the reducing atmosphere. These Co NPs serve as catalyst/active sites for growth of CNTs, and because of this growth Co NPs are wrapped inside CNTs. With longer plasma exposure, more CNTs emerge from the polyhedrons and become the substrate for more EOG growth. Thus, EOG becomes the dominant surface feature in sample C-ZIF/SS-8.

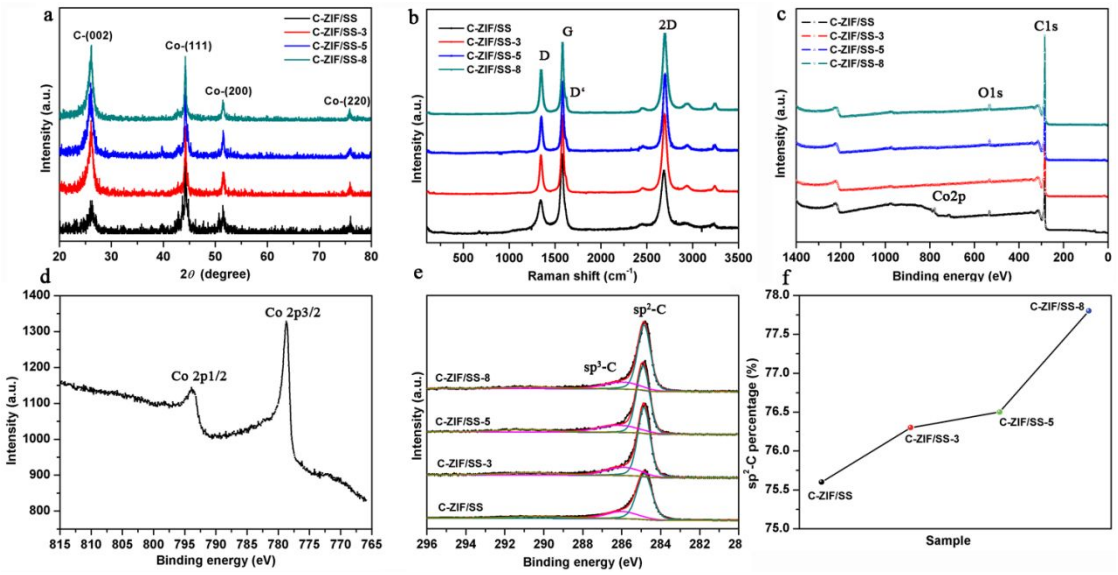

Figure 2. XRD patterns (a), Raman spectra (b),and XPS survey spectra (c) of different samples. XPS Co2p high resolution spectrum of C-ZIF/SS (d), XPS C1s high resolution spectra of different samples (e) and the percentage of sp^2 carbon in different samples (f).

X-ray powder diffraction (XRD) patterns of different samples are exhibited in Figure 2(a). The sharp diffraction peak located at ~26° 2θ for three plasma-exposed samples arises from the (111) crystal plane of graphene, CNTs and carbonized ZIF, demonstrating their well graphitized structure.[34-35] Without EOG and CNTs deposition in the sample shielded from the plasma, this peak has considerably lower intensity for sample C-ZIF/SS. Other XRD peaks are assigned to (111), (200) and (220) crystal planes of metallic Co with fcc structure, and this is consistent with the SAED pattern(Figure 1(g)).[36] Other differences between plasma-treated samples and sample C-ZIF/SS are revealed by Raman spectra (Figure 2(b)). Raman peaks located at 1349, 1587 and 2701 cm^{-1} are assigned to the D, G and 2D bands of graphite materials, representing breathing mode of sp^2 carbon rings, planar

configuration sp^2 bonded carbon and a second order of the D band (or an overtone of the D band), respectively.[37] The D´ band can also be observed for three plasma-treated samples due to the presence of exposed graphene edges. The ratio of I_D and I_G increases slightly with the plasma treatment time. This is ascribed to the increased amount of graphene edges. Raman peaks of metallic Co (i.e., peaks at 470 and 675 cm^{-1}) can be discerned in sample C-ZIF/SS(Figure S5) but are undetectable in the plasma-treated samples. This suggests that Co NPs are buried in the carbon layers,[38] as revealed by HRTEM in Figure S4(a). Compared to the exposed Co NPs, Co NPs buried in carbon were stable even in the used oxidizing electrolyte (6 M aqueous KOH solution) and at high voltage exceeding their oxidation potential, as confirmed in the electrochemical tests.

The surface chemical states of different samples were analyzed by X-ray photoelectron spectroscopy (XPS), and the results are represented in Figure 2(c-f). Except for sample C-ZIF/SS, showing the C1s, O1s and Co2p peaks, other samples show only the C1s and O1speaks (Figure 2(c)).This is in accord with Raman results for the Co-encapsulating carbon structure in these samples. Well-defined Co $2p_{3/2}$ (binding energy (BE) = 778.5 eV) and Co $2p_{1/2}$ (BE = 793.5 eV) peaks further demonstrate the metallic state of Co nanoparticles in sample C-ZIF/SS (Figure 2(d)).[39] The nature of carbon bonds in the carbonized samples is revealed in the high resolution C 1s spectra (Figure 2(e)). These samples are composed of sp^2 (BE = 284.8 eV) and sp^3 (BE = 285.9 eV) hybridized carbon atoms, whose ratio can be used to estimate the conductivity of carbon materials.[40] As shown in Figure 2(f), samples with EOG and CNTs have a higher percentage of sp^2 carbon

(more than 75%) than sample C-ZIF/SS with CNTs only. This suggests the high conductivity for the plasma carbonized samples.

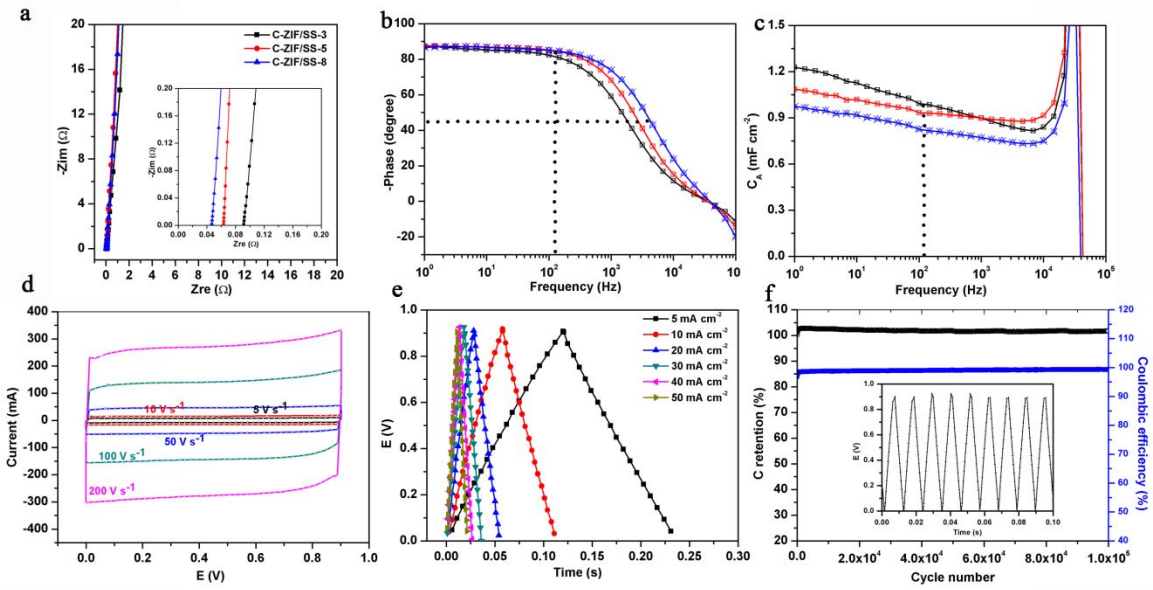

Figure 3. Nyquist spectra (inset shows the high-frequency region) (a), Bode diagrams (b) and areal capacitance *vs.* frequency plots (c) for different electrode materials in 6 M aqueous KOH electrolyte. CV curves for different scan rates (d), GCD profiles for different current densities (e), and plots of capacitance retention and coulombic efficiency within half million GCD cycles at 50 mA cm^{-2}(inset shows part of GCD curves) (f) for sample C-ZIF/SS-5 in 6 M aqueous KOH electrolyte.

To characterize the electrochemical properties of three plasma-treated electrodes, symmetric coin cells were assembled using 6 M aqueous KOH electrolyte. The cell performances were investigated using electrochemical impedance spectroscopy (EIS),

cyclic voltammetry (CV), and galvanostatic charge-discharge (GCD) methods. Figure 3(a) shows the Nyquist plot of the acquired EIS spectra from three plasma-treated samples. The impedance spectra resemble a nearly vertical line. The commonly observed 45^{o} tilted line region as a sign of characteristic of the distributed porous effect cannot be discerned in these spectra. This suggests the EOG cluster-forming nanostructures, with straightforward, shallow and wide opening channels between the vertical graphene sheets, do not exhibit the distributed mesoporous effect, and therefore do not restrict the subsequent electrical double layer capacitance (EDLC) formation rate. The impedance spectra also do not present the typical semicircle feature, which is the signature of a significant interface resistance between the electrode material and the current collector. This is justifiable since ZIF-67 was directly deposited and subsequently carbonized on a SS current collector, and hence they are in the intimate contact with negligible interface resistance. As a result, the nearly vertical impedance line directly intersects the resistance (Zre) axis at an angle close to 90^{o}, giving an equivalent serial resistance (ESR) less than 0.1 Ω (e.g., less than 0.05 Ω for sample C-ZIF/SS-8). This small ESR includes contribution of the electrode material itself, further confirming a high conductivity of the C-ZIF structure, especially the structure obtained after 8 minutes of the plasma treatment. With such a small ESR, the cell could be charged and discharged at very high rates with minimum internal loss.

The Bode plots of the EIS spectra give their phase angle variation as a function of the increasing frequency (Figure 3(b)). Two important characteristics, the phase angle at 120 Hz (φ_{120}) and the frequency at the phase angle of -45^{o} (f_0), can be extracted to evaluate the

electrode performances. As shown in Figure 3(b), all plasma-treated samples have an excellent frequency response. For the C-ZIF/SS-3-, C-ZIF/SS-5-, and C-ZIF/SS-8-based cells, the φ_{120} and the f_0 are ~-80° and 1.7 KHz, ~-84° and 2.7 KHz, and ~-85° and 4.1 KHz, respectively. The areal capacitance (C_A) of each electrode is plotted against frequency in Figure 3(c). Although the C-ZIF/SS-3 electrode has the highest C_A among all electrodes at a frequency below 1 kHz, the C_A of the C-ZIF/SS-5 electrode surpasses the C_A of two other electrodes at a frequency above 1 KHz, and this capacitance is maintained at more than 0.85 mF cm^{-2} until 10 kHz. Specifically, the C_A at 120 Hz (C_A^{120}), another important parameter used to evaluate the performance of HF-ECs, is ~1.02, ~0.95 and ~0.83 mF cm^{-2} for the C-ZIF/SS-3, C-ZIF/SS-5 and C-ZIF/SS-8 electrodes, respectively.

For comparative purposes, sample C-ZIF/SS, i.e., the sample not directly exposed to CH_4/H_2 plasma and hence without deposited EOG, was tested under the same experimental conditions, and the results are presented in Figure S6. Even though this electrode-based cell also has a small ESR (~0.1 Ω), its impedance spectrum is more tilted (Figure S6(a)), compared to a nearly vertical lines obtained for the impedance spectra of samples directly exposed to the plasma (Figure 3(a)). Thus, the C-ZIF/SS-based cell behaves more like a constant phase element, than an ideal capacitor. Its φ_{120} and f_0 are only ~-68° and 570 Hz, respectively (Figure S6(b)). The slow response from sample C-ZIF/SS could be caused by some micro- or meso-pores formed during carbonization, whereas in three other samples the access to such pores is blocked by EOG encapsulation. These results clearly demonstrate the importance of the unique structure produced by the plasma treatment in

affecting the electrochemical performance of the resulting cells.

Sample C-ZIF/SS-5 was tested using CV technique. As shown in Figure 3(d), CV curves exhibit rectangular shape for scan rates up to 200 V s^{-1} and maintain quasi-rectangular shape at the scan rate of 1000 V s^{-1}. This is due to the extremely low electronic resistance and the absence of micro-, dead or tortuous pores throughout the electrode. The current density vs. the scan rate is approximately a linear relationship (Figure S7(a)). The C_A was calculated using equations given in the Experimental section, and the resulting values were plotted as a function of scan rate. The C_A value decreases only slightly for larger scan rates, even for the values as large as 1000 V s^{-1}, which agrees well with the EIS results (Figure S7(b)).

The rate capability and the long-term stability of the C-ZIF/SS-5 electrode-based cells were also tested by GCD method. The GCD curves collected for different current densities (Figure 3(e)) have triangular shape (the IR drop at the beginning of discharge is negligible), reflecting this electrode's extraordinary capacitive properties. With the high-rate performance, its capacitance decreases only slightly as the GCD current increases. At a current density of 100 mA cm^{-2}, the capacitance still retains ~80% of the value obtained at a low current density (Figure S8). In the GCD cycling stability test under the current density of 50 mA cm^{-2}, the capacitance retention is ~100% within half million cycles, clearly demonstrating electrodes' excellent potential for long-term stability.

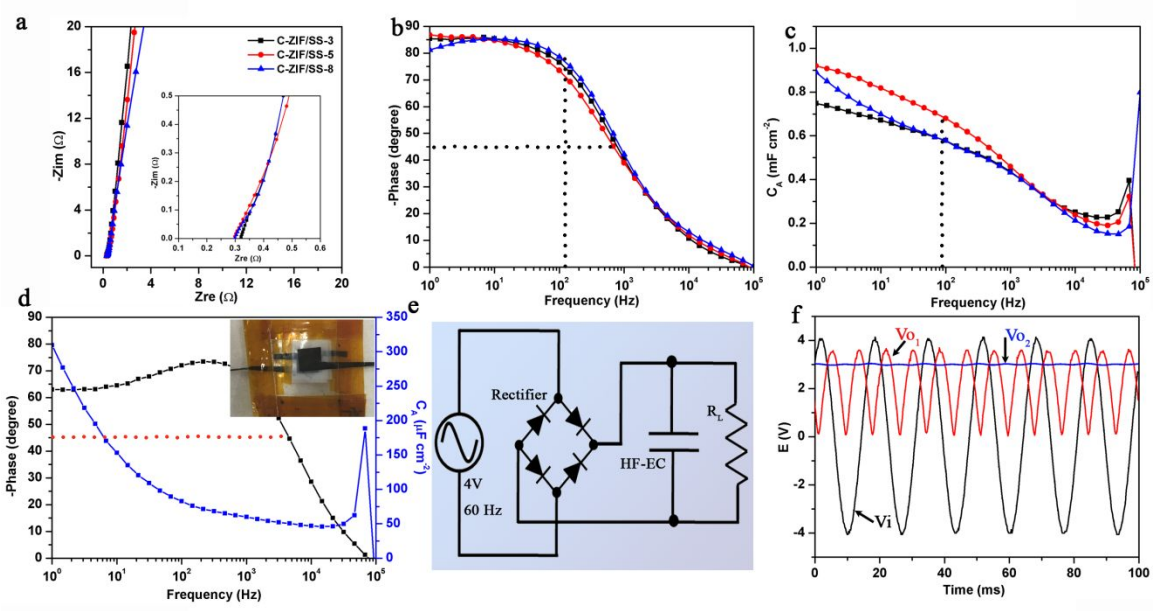

Figure 4. Nyquist spectra (inset shows the high-frequency region) (a), Bode diagrams (b) and areal capacitance *vs.* frequency plots (c) for different electrode materials in 1 M $TEABF_4$ electrolyte. Bode diagram and capacitance vs. frequency plot for the stacked cell (inset shows a photo of the stacked cell) (d). AC/DC converter circuit (e).The input (Vi) and output voltages with (Vo_2) and without (Vo_1) HF-EC involved (f).

Because of water decomposition, the highest applicable cell voltage is ~0.9 V when using water-based electrolytes. To expand the testing voltage window, organic electrolyte, 1 M tetraethylammonium tetrafluoroborate ($TEABF_4$) in acetonitrile (AN), was used to evaluate the electrochemical performances of these electrodes. In comparison to that of the aqueous-based electrolyte, the conductivity of $TEABF_4$/AN solution is much lower, causing the ESR to increase to ~0.3 Ω (Figure 4(a)). Different from Nyquist plots of electrodes using 6 M aqueous KOH as electrolyte, a transition part, comprised of a more

titled line, is observed for the organic cell (the inset of Figure 4(a)). This suggests a relatively slow electrolytic ion moving speed within the electrode, which may be due to the large size of the ions provided by $TEABF_4$. Bode diagrams are shown in Figure 4(b), and all electrodes tested gave the f_0 of ~1 KHz and the φ_{120} of ~-75°. The C-ZIF/SS-5-based electrode has the highest areal capacitance of ~0.75 mF cm^{-2} at 120 Hz (Figure 4(c)). As an example, the real and imaginary components of the complex capacitance and their dependence on frequency as well as CV curves obtained for different scan rates for the C-ZIF/SS-8-based cell are presented in Figure S9. These results agree with the aforementioned EIS analysis.

As a proof of concept, the 7.5 V cell was fabricated by integrating three pairs of electrodes together into one cell. Nickel foil was used as the substrate to grow ZIF-67 (Figure S10). Promisingly, this cell showed the φ_{120} of ~-72° and the f_0 of 3.8 KHz (Figure 4(d)). Although the C_A^{120} was only ~75 μF cm^{-2} (Figure 4(d)), this value is still much higher than these reported when using passivated or dielectric layers to increase the voltage.[41-42] As shown in Figure S11(a), the electrolyte is stable within the 7.5 V window. In this preliminary demonstration of an integrated cell, the ESR was very high (Figure S11(b)), since it has not been optimized; and a better performance is expected in the future. Decrease of the ESR of the integrated cell should increase its capacitance and frequency response.

One organic HF-EC cell was applied as a filtering capacitor for the line-frequency AC/DC conversion (Figure 4(e)). A 60 Hz 4V AC voltage was used as the input source. The AC input voltage first passed a full-wave rectifier before feeding the filtering capacitor.

As shown in Figure 4(f), a stable ~3.0 V DC voltage was successfully obtained after rectification and filtering. This confirms the potential of the carbonized ZIF-67-based HF-ECs for ripple current filtering applications.

Conclusions

To fabricate the high-performance electrodes, the EOG/CNT/C-ZIF-67 composites were successfully prepared on metal substrates from ZIF-67 precursors through their rapid carbonization in a PECVD process. This resulted in a carbonized particulate ZIF-67 skeleton with the EOG and CNTs formed around it. The composite electrodes with a structure built by the carbonized ZIF-67 particles, Co NPs, EOG and CNTs showed excellent electron conductivity and adequate surface area, resulting in cells with very good frequency response and large specific capacitance in both inorganic and organic electrolytes. To increase the applicable voltage for practical applications, an integrated cell having three pairs of electrodes stacked together, was fabricated as a proof of concept, and this cell showed a stable potential window of 7.5 V and a characteristic frequency in the kHz range.

Experimental section

Material synthesis

Stainless steel (SS) disks (0.5 mm), used in coin cells as the current collectors, were polished and then ultrasonically washed, first in deionized water and then in acetone. Solution 1 was prepared by dissolving 0.320 g of 2-methylimidazole 25 mL of methanol. Solution 2 was prepared by dissolving 0.295 g of cobalt nitrate hexahydrate in 25 mL of methanol. After immersing the SS disk in solution1 that was earlier poured into a reactor, solution 2 was added quickly, and the reactor was sealed, transferred into the oven and heated at 40 ^{o}C for 24 h. To increase the amount of ZIF-67 deposited on the SS disk, the above procedure was repeated using the SS disk recovered from the first synthesis. The obtained ZIF-67 film samples were washed with methanol and dried in an oven at 80 ^{o}C overnight.

The ZIF samples were placed onto the molybdenum holder and transferred to the heating stage in a PECVD system. After the chamber was evacuated, hydrogen (100 sccm) and methane (50 sccm) were introduced into the chamber, and the pressure was maintained at 30 Torr. The heating temperature was then increased to 750 ^{o}C, and 1 kW microwave radiation was applied to create plasma. The detailed procedure can be found in our previous work.[4] Different plasma treatment durations (3, 5 and 8 minutes) were applied here to study the structural evolution of products, and the resulting samples are designated as C-ZIF/SS-3, C-ZIF/SS-5 and C-ZIF/SS-8, respectively. For comparison, the ZIF was also sandwiched between graphite sheets to protect it from the direct exposure to the plasma, and treated in

the plasma for 5 minutes without changing other experimental conditions. This sample is designated as C-ZIF/SS.

Materials Characterization

The structures and morphologies of all samples were visualized using field emission scanning electron microscopy (FE-SEM, Supra35, Gemini) and transmission electron microscopy (TEM, H-9500, Hitachi). The crystal structure was identified using X-ray powder diffraction (XRD, Ultima Ⅲ, Rigaku). The surface chemical states and chemical bonds were characterized using X-ray photoelectron spectroscopy (XPS, 5000 VersaProbe, PHI) and Raman spectroscopy (532 nm excitation laser, SENTERRA, Bruker Optics).

Electrochemical Measurements

Symmetric coin cells were employed to study the electrochemical performances of different samples. 6 M aqueous KOH solution was used as inorganic electrolyte paired with Celgard 3501 separator.1 M tetraethylammonium tetrafluoroborate ($TEABF_4$) in anhydrous acetonitrile (AN) solution was used as organic electrolyte paired with commercial Celgard 2325 separator. The area of each electrode was 1.96 cm^2. Cells with organic electrolyte were assembled in the Argon-filled glovebox having water and oxygen content less than 0.1 ppm. All measurements were carried out on a Biologic SP-150 electrochemical workstation. Cyclic voltammetry (CV) curves were obtained within the potential windows of 0-0.9 V and 0-2.5 V for inorganic and organic electrolytes, respectively, using scan rates up to 1000 V s^{-1}. Electrochemical impedance spectroscopy (EIS) was performed in the frequency range 100 kHz – 1 Hz with 10 mV AC signal.

Galvanostatic charge-discharge (GCD) tests were conducted under different current densities ranging from 10 to 100 mA cm^{-2}.

The areal specific capacitance (C_A) of different electrodes was calculated from EIS spectra using equations (1) and (2):

$$C(f) = \frac{-1}{2\pi f Z''(f)} \quad (1)$$

$$C_A(f) = 2C(f)/A \quad (2)$$

Where *f* is the frequency, Z" is the imaginary part of the impedance and A is the area of a single electrode.

The frequency dependent capacitance can be evaluated using equations(3-5):

$$C = C' - jC'' \quad (3)$$

$$C' = \frac{-Z''}{2\pi|Z|^2} \quad (4)$$

$$C'' = \frac{Z'}{2\pi|Z|^2} \quad (5)$$

Where C' and C" correspond to the actual capacitance and capacitance losses due to the resistance, respectively. The areal capacitances of a single electrode were further calculated as $C'_A = 2C'(f)/A$ and $C''_A = 2C''(f)/A$.

The CV and GCD results were also used to analyze the capacitor performances. For CV curves, the electrode capacitance was calculated using equation (6):

$$C_A = S/(v * \Delta E) \quad (6)$$

Where S is the integrated area under the CV curve, *v* is the scan rate and ΔE is the scan

voltage range.

In order to integrate three separated HF-ECs in one package to get a cell with 7.5 V working voltage, ZIF-67 was first grown on Ni foil (20 μm, area: 1 cm^2) instead of SS spacer considering the flexibility and manageability of Ni foil. The following carbonization and VOG modification processes were the same as they were carried out for ZIF-67 covered SS spacer samples. Celgard 2325 film and 1 M tetraethylammonium tetrafluoroborate ($TEABF_4$) in anhydrous acetonitrile (AN) solution were used as separator and electrolyte, respectively. These three single HF-ECs connected in serials were isolated by and sealed in thermoplastic films (as shown in the schematic in Figure S10).

Acknowledgements

This work was supported by National Science Foundation (1611060, 1820098).

Supplementary Information

Digital photo showing the ZIF-67 film before and after being treated in PECVD system. SEM and TEM images of different samples, Raman spectrum, CV, EIS and GCD results.

References

1. Miller, J. R.; Outlaw, R. A.; Holloway, B. C., Graphene double-layer capacitor with ac line-filtering performance. *Science* **2010,** *329* (5999), 1637-9.
2. Fan, Z. Y.; Islam, N.; Bayne, S. B., Towards kilohertz electrochemical capacitors for filtering and pulse energy harvesting. *Nano Energy* **2017,** *39*, 306-320.
3. Cai, M. Z.; Outlaw, R. A.; Quinlan, R. A.; Premathilake, D.; Butler, S. M.; Miller, J. R., Fast Response, Vertically Oriented Graphene Nanosheet Electric Double Layer Capacitors Synthesized from C2H2. *ACS Nano* **2014,** *8* (6), 5873-5882.
4. Islam, N.; Warzywoda, J.; Fan, Z. Y., Edge-Oriented Graphene on Carbon Nanofiber for High-Frequency Supercapacitors. *Nano-Micro Lett.* **2018,** *10* (1), 8.
5. Ren, G. F.; Pan, X.; Bayne, S.; Fan, Z. Y., Kilohertz ultrafast electrochemical supercapacitors based on perpendicularly-oriented graphene grown inside of nickel foam. *Carbon* **2014,** *71*, 94-101.
6. Zhu, Y. W.; Murali, S.; Stoller, M. D.; Ganesh, K. J.; Cai, W. W.; Ferreira, P. J.; Pirkle, A.; Wallace, R. M.; Cychosz, K. A.; Thommes, M.; Su, D.; Stach, E. A.; Ruoff, R. S., Carbon-Based Supercapacitors Produced by Activation of Graphene. *Science* **2011,** *332* (6037), 1537-1541.
7. Wu, Z. S.; Liu, Z. Y.; Parvez, K.; Feng, X. L.; Mullen, K., Ultrathin Printable Graphene Supercapacitors with AC Line-Filtering Performance. *Adv. Mater.* **2015,** *27* (24), 3669-3675.
8. Nathan-Walleser, T.; Lazar, I. M.; Fabritius, M.; Tolle, F. J.; Xia, Q.; Bruchmann, B.; Venkataraman, S. S.; Schwab, M. G.; Mulhaupt, R., 3D Micro-Extrusion of Graphene-based Active Electrodes: Towards High-Rate AC Line Filtering Performance Electrochemical Capacitors. *Adv. Funct. Mater.* **2014,** *24* (29), 4706-4716.
9. Lin, J.; Zhang, C. G.; Yan, Z.; Zhu, Y.; Peng, Z. W.; Hauge, R. H.; Natelson, D.; Tour, J. M., 3-Dimensional Graphene Carbon Nanotube Carpet-Based Microsupercapacitors with High Electrochemical Performance. *Nano Lett.* **2013,** *13* (1), 72-78.
10. Sheng, K. X.; Sun, Y. Q.; Li, C.; Yuan, W. J.; Shi, G. Q., Ultrahigh-rate supercapacitors based on eletrochemically reduced graphene oxide for ac line-filtering. *Sci Rep* **2012,** *2*, 5.
11. Bo, Z.; Xu, C.; Yang, H.; Shi, H.; Yan, J.; Cen, K.; Ostrikov, K., Hierarchical, Vertically-Oriented Carbon Nanowall Foam Supercapacitor Using Room Temperature Ionic Liquid Mixture for AC Line Filtering with Ultrahigh Energy Density. *ChemElectroChem* **2019,** *6* (8), 2167-2173.
12. Rangom, Y.; Tang, X.; Nazar, L. F., Carbon Nanotube-Based Supercapacitors with Excellent ac Line Filtering and Rate Capability via Improved Interfacial Impedance. *ACS Nano* **2015,** *9* (7), 7248-7255.
13. Yoo, Y.; Kim, S.; Kim, B.; Kim, W., 2.5 V compact supercapacitors based on ultrathin carbon nanotube films for AC line filtering. *J. Mater. Chem. A* **2015,** *3* (22), 11801-11806.
14. Yoo, Y.; Kim, M. S.; Kim, J. K.; Kim, Y. S.; Kim, W., Fast-response supercapacitors with graphitic ordered mesoporous carbons and carbon nanotubes for AC line filtering. *J. Mater. Chem. A* **2016,** *4* (14), 5062-5068.
15. Li, Q.; Sun, S.; Smith, A. D.; Lundgren, P.; Fu, Y.; Su, P.; Xu, T.; Ye, L.; Sun, L.; Liu, J., Compact and low loss electrochemical capacitors using a graphite/carbon nanotube hybrid material for miniaturized systems. *Journal of Power Sources* **2019,** *412*, 374-383.
16. Islam, N.; Li, S. Q.; Ren, G. F.; Zu, Y. J.; Warzywoda, J.; Wang, S.; Fan, Z. Y., High-frequency electrochemical capacitors based on plasma pyrolyzed bacterial cellulose aerogel for current ripple filtering and pulse energy storage. *Nano Energy* **2017,** *40*, 107-114.

17. Kossyrev, P., Carbon black supercapacitors employing thin electrodes. *Journal of Power Sources* **2012,** *201*, 347-352.

18. Islam, N.; Wang, S.; Warzywoda, J.; Fan, Z. Y., Fast supercapacitors based on vertically oriented MoS2 nanosheets on plasma pyrolyzed cellulose filter paper. *Journal of Power Sources* **2018,** *400*, 277-283.

19. Wu, Z. S.; Feng, X. L.; Cheng, H. M., Recent advances in graphene-based planar micro-supercapacitors for on-chip energy storage. *Natl. Sci. Rev.* **2014,** *1* (2), 277-292.

20. Kurra, N.; Jiang, Q.; Syed, A.; Xia, C.; Alshareef, H. N., Micro-Pseudocapacitors with Electroactive Polymer Electrodes: Toward AC-Line Filtering Applications. *ACS Appl. Mater. Interfaces* **2016,** *8* (20), 12748-12755.

21. Xu, S.; Liu, W.; Hu, B.; Wang, X., Circuit-integratable high-frequency micro supercapacitors with filter/oscillator demonstrations. *Nano Energy* **2019,** *58*, 803-810.

22. Gund, G. S.; Park, J. H.; Harpalsinh, R.; Kota, M.; Shin, J. H.; Kim, T.-i.; Gogotsi, Y.; Park, H. S., MXene/Polymer Hybrid Materials for Flexible AC-Filtering Electrochemical Capacitors. *Joule* **2019,** *3* (1), 164-176.

23. Sellam, A.; Jenjeti, R. N.; Sampath, S., Ultrahigh-Rate Supercapacitors Based on 2-Dimensional, 1T MoS2 x Se2 (1–x) for AC Line-Filtering Applications. *The Journal of Physical Chemistry C* **2018,** *122* (25), 14186-14194.

24. Wu, Z. K.; Li, L. Y.; Lin, Z. Y.; Song, B.; Li, Z.; Moon, K. S.; Wong, C. P.; Bai, S. L., Alternating current line-filter based on electrochemical capacitor utilizing template-patterned graphene. *Sci Rep* **2015,** *5*, 7.

25. Liu, W. W.; Lu, C. X.; Li, H. L.; Tay, R. Y.; Sun, L. M.; Wang, X. H.; Chow, W. L.; Wang, X. L.; Tay, B. K.; Chen, Z. W.; Yan, J.; Feng, K.; Lui, G.; Tjandra, R.; Rasenthiram, L.; Chiu, G.; Yu, A. P., Paper-based all-solid-state flexible micro-supercapacitors with ultra-high rate and rapid frequency response capabilities. *J. Mater. Chem. A* **2016,** *4* (10), 3754-3764.

26. Chen, C.; Cao, J.; Wang, X. Y.; Lu, Q. Q.; Han, M. M.; Wang, Q. R.; Dai, H. T.; Niu, Z. Q.; Chen, J.; Xie, S. S., Highly stretchable integrated system for micro-supercapacitor with AC line filtering and UV detector. *Nano Energy* **2017,** *42*, 187-194.

27. Chen, Y. Q.; Zhang, X. N.; Xie, Z. P., Flexible Nitrogen Doped SiC Nanoarray for Ultrafast Capacitive Energy Storage. *ACS Nano* **2015,** *9* (8), 8054-8063.

28. Miller, J. R.; Outlaw, R. A., Vertically-Oriented Graphene Electric Double Layer Capacitor Designs. *J. Electrochem. Soc.* **2015,** *162* (5), A5077-A5082.

29. Yang, P. H.; Chao, D. L.; Zhu, C. R.; Xia, X. H.; Zhang, Y. Q.; Wang, X. L.; Sun, P.; Tay, B. K.; Shen, Z. X.; Mai, W. J.; Fan, H. J., Ultrafast-Charging Supercapacitors Based on Corn-Like Titanium Nitride Nanostructures. *Adv. Sci.* **2016,** *3* (6), 7.

30. Ren, G.; Hoque, M. N. F.; Pan, X.; Warzywoda, J.; Fan, Z., Vertically aligned VO 2 (B) nanobelt forest and its three-dimensional structure on oriented graphene for energy storage. *J. Mater. Chem. A* **2015,** *3* (20), 10787-10794.

31. Torad, N. L.; Salunkhe, R. R.; Li, Y. Q.; Hamoudi, H.; Imura, M.; Sakka, Y.; Hu, C. C.; Yamauchi, Y., Electric Double-Layer Capacitors Based on Highly Graphitized Nanoporous Carbons Derived from ZIF-67. *Chem.-Eur. J.* **2014,** *20* (26), 7895-7900.

32. Zhang, W.; Jiang, X. F.; Wang, X. B.; Kaneti, Y. V.; Chen, Y. X.; Liu, J.; Jiang, J. S.; Yamauchi, Y.; Hu, M., Spontaneous Weaving of Graphitic Carbon Networks Synthesized by Pyrolysis of ZIF-67 Crystals. *Angew.*

Chem.-Int. Edit. **2017,** *56* (29), 8435-8440.

33. Bala, T.; Arumugam, S. K.; Pasricha, R.; Prasad, B. L. V.; Sastry, M., Foam-based synthesis of cobalt nanoparticles and their subsequent conversion to CocoreAgshell nanoparticles by a simple transmetallation reaction. *J. Mater. Chem.* **2004,** *14* (6), 1057-1061.

34. Zhang, J. L.; Yang, H. J.; Shen, G. X.; Cheng, P.; Zhang, J. Y.; Guo, S. W., Reduction of graphene oxide via L-ascorbic acid. *Chem. Commun.* **2010,** *46* (7), 1112-1114.

35. Chen, W. F.; Yan, L. F.; Bangal, P. R., Preparation of graphene by the rapid and mild thermal reduction of graphene oxide induced by microwaves. *Carbon* **2010,** *48* (4), 1146-1152.

36. Du, M.; Liu, Q. W.; Huang, C. J.; Qiu, X. Q., One-step synthesis of magnetically recyclable Co@BN core-shell nanocatalysts for catalytic reduction of nitroarenes. *RSC Adv.* **2017,** *7* (56), 35451-35459.

37. Malard, L. M.; Pimenta, M. A.; Dresselhaus, G.; Dresselhaus, M. S., Raman spectroscopy in graphene. *Phys. Rep.-Rev. Sec. Phys. Lett.* **2009,** *473* (5-6), 51-87.

38. Dai, X. P.; Li, Z. Z.; Ma, Y. D.; Liu, M. Z.; Du, K. L.; Su, H. X.; Zhuo, H. Y.; Yu, L.; Sun, H.; Zhang, X., Metallic Cobalt Encapsulated in Bamboo-Like and Nitrogen-Rich Carbonitride Nanotubes for Hydrogen Evolution Reaction. *ACS Appl. Mater. Interfaces* **2016,** *8* (10), 6439-6448.

39. Su, Y. H.; Zhu, Y. H.; Jiang, H. L.; Shen, J. H.; Yang, X. L.; Zou, W. J.; Chen, J. D.; Li, C. Z., Cobalt nanoparticles embedded in N-doped carbon as an efficient bifunctional electrocatalyst for oxygen reduction and evolution reactions. *Nanoscale* **2014,** *6* (24), 15080-15089.

40. Hirono, S.; Umemura, S.; Tomita, M.; Kaneko, R., Superhard conductive carbon nanocrystallite films. *Appl. Phys. Lett.* **2002,** *80* (3), 425-427.

41. Romann, T.; Oll, O.; Pikma, P.; Kirsimae, K.; Lust, E., 4-10 V capacitors with graphene-based electrodes and ionic liquid electrolyte. *Journal of Power Sources* **2015,** *280*, 606-611.

42. Romann, T.; Oll, O.; Pikma, P.; Tamme, H.; Lust, E., Surface chemistry of carbon electrodes in 1-ethyl-3-methylimidazolium tetrafluoroborate ionic liquid - an in situ infrared study. *Electrochim. Acta* **2014,** *125*, 183-190.

Table of Content (ToC)